Ribeka Takahashi
Graduate Research Assistant
e-mail: ribekat@byu.net

Dikshya Prasai
Undergraduate Research Assistant
e-mail: pdikshya@gmail.com

Brent L. Adams
Dusenberry Professor
e-mail: b_l_adams@byu.edu

Christopher A. Mattson
Assistant Professor
e-mail: mattson@byu.edu

Department of Mechanical Engineering,
Brigham Young University,
Provo, Utah 84602

Hybrid Bishop-Hill Model for Elastic-Yield Limited Design With Non-orthorhombic Polycrystalline Metals

A method is presented for adapting the classical Bishop-Hill model to the requirements of elastic/yield-limited design in metals of arbitrary crystallographic texture. The proposed Hybrid Bishop-Hill (HBH) model, which will be applied to ductile FCC metals, retains the "stress corners" of the polyhedral Bishop-Hill yield surface. However, it replaces the 'maximum work criterion' with a criterion that maximizes the projection of the applicable local corner stress state onto the macroscopic stress state. This compromise leads to a model that is much more accessible to yield-limited design problems. Demonstration of performance for the HBH model is presented for an extensive database for oxygen free electronic copper. The design problem considered is a hole-in-a-plate configuration of thin sheets loaded in uniaxial tension in arbitrary directions relative to the principal directions of material orthorhombicity. Results obtained demonstrate that HBH-based elastic/yield limited design is capable of predicting complex and highly non-intuitive behaviors, even within standard problems. [DOI: 10.1115/1.4004829]

1 Introduction

Three fundamental and interrelated design parameters affect yielding in materials; they are (1) part geometry, (2) material microstructure, and (3) boundary conditions. In typical design practice, these three types of design parameters lead to specific stress states, which are then compared with simplified yield criteria (e.g., von-Mises and Tresca criteria) as a means to predict failure. Even simpler, in the most practiced sense, the largest stress component in a part is compared to a measured yield strength (typically recovered from the standard uniaxial tensile test). Clearly this simple yield-limited approach has been used in the past to create great parts and products [1,2]. However, for any material that is not isotropic and homogenous, these methods rely upon an over simplification of the yield surface. Reliance upon this simplified approach in yield-limited design is partially due to ready-accessible tabulated yield strength data. But its use typically implies negligible variation of the yield strength with direction in the material. Extending these data sets to include yield anisotropy can be very challenging, and has only been attempted in the most highly constrained design problems. Ultimately, the readily available minimal yield data reduces the design engineer's opportunity to search for optimal material performance, which can only be done by including property anisotropy. This paper presents a new, and accessible model for the anisotropic yield surface that can be used to consider first-order anisotropic yield characteristics in design.

The literature provides useful insight into the evaluation and representation of anisotropic yield surface models [3–5]. Through adaptations of the Von Mises yield criteria, an empirical representation of the anisotropic yield surface can be developed. This representation, however, typically assumes material orthrombicity, and requires parameters that can only be found through implementation of a significant testing program. Several microstructure-based theories have been offered for the prediction of yielding in polycrystalline materials, such as the Taylor model [6], the Bishop-Hill model, [7,8] and various intermediate or hybrid models [9]. These classical models are focused upon integrating crystallographic texture (preferred distribution of lattice orientations) into yield predictions. Typically they require the input of a *critical resolved shear stress*, in order to properly scale the predictions to measured yield properties.

It is important to note that under the classical Taylor [6] and Bishop-Hill [7,8] methodologies, plastic strain states must be specified in order to evaluate the yield stress. The difficulty is that, for design problems focused upon initial yielding, the elastic and plastic components of the total strain are comparable in magnitude and difficult to separate. Thus, the precise condition of plastic strain at initial yielding is not precisely specified. It follows that application of these classical microstructure-based theories of plasticity to initial yielding is a rather imperfect approximation at best.

The new models presented in this work, called the Hybrid Bishop-Hill (HBH) model, is closely related to the classical Bishop-Hill model [7,8] in predicting local stress states and mechanical yielding. The HBH model has the advantage, when used in the context of part design, of greatly expanding the design space, thus enabling the designer to reach into traditionally unexplored areas of performance. Because the computational burden associated with the full characterization of the five-dimensional anisotropic yield surface is prohibitive, we develop a reduced representation of the yield surface that is much more accessible. Typically only a small portion of the complete yield surface is required for part design and the HBH model facilitates rapid access to the pertinent domain of the yield surface

This paper (1) describes a stress-focused anisotropic yield limited design approach, incorporating the new HBH model, which (2) does not require an evaluation of plastic strain (or strain rate) at yielding, (3) preserves the characteristic of local grain-scale heterogeneity present in the Taylor and Bishop-Hill models, and (4) efficiently accesses a realistic portion of the anisotropic yield surface pertinent to the mechanical design.

The new methodology is applied to an extensive database of rolled and annealed FCC Cu materials (Oxygen Free Electronic purity grade). Although these materials exhibit the typical orthorhombic symmetry in their crystallographic textures, consideration is also given to rigid body rotations of the principal axes of

Contributed by the Materials Division of ASME for publication in the JOURNAL OF ENGINEERING MATERIALS AND TECHNOLOGY. Manuscript received April 8, 2011; final manuscript received July 29, 2011; published online December 6, 2011. Assoc. Editor: Hussein Zbib.

orthorhombicity, about the rolling plane normal direction. Property closures, of the type developed by microstructure-sensitive design methodology, [10,11] are utilized to describe the breadth of elastic/yielding performance available within the complete material database. Demonstration of the new methodology is focused upon the common problem of stress concentration about a circular hole in a plate, loaded under uniaxial tension in arbitrary directions with respect to the principal material axes. Analytical solutions to the elastic equilibrium equations, provided by Lekhnitskii [12] are used in the mechanical analysis.

The reminder of this paper is presented as follows. In Sec. 2, we present the technical preliminaries required to introduce the new methodology. In Sec. 3, we present the new approach for the mechanical yield limit design. Section 4 presents the application of the approach to the hole-in-the-plate design problem.

2 Background

2.1 Property Closure. The simplest form of homogenization relations, associating the distribution of local states of microstructure to estimates of the macroscopic (effective) elasticity, require only volume fraction information on the distribution. Hill-Paul upper- and lower-bounds [Fullwood 2010] on the stored elastic strain energy density can be expressed in the following ways:

$$\begin{aligned}\bar{\varepsilon}_{ij}(\bar{S})^{-1}_{ijkl}\bar{\varepsilon}_{kl} \le \bar{\varepsilon}_{ij}C^{\text{eff}}_{ijkl}\bar{\varepsilon}_{kl} \le \bar{\varepsilon}_{ij}\bar{C}_{ijkl}\bar{\varepsilon}_{kl}\\ \bar{\varepsilon}_{ij}(\bar{C})^{-1}_{ijkl}\bar{\varepsilon}_{kl} \le \bar{\varepsilon}_{ij}S^{\text{eff}}_{ijkl}\bar{\varepsilon}_{kl} \le \bar{\varepsilon}_{ij}\bar{S}_{ijkl}\bar{\varepsilon}_{kl}\end{aligned} \tag{1}$$

Here C^{eff} and S^{eff} are the fourth-order effective elastic stiffness and compliance tensors, S and C are the local ones, ε is the local (second-order) infinitesimal strain tensor, σ is the Cauchy stress tensor, and the bar over the top of any of these tensors indicates the volume average of the same. (Note that the Einstein summation convention has been used in Eq. (1), in that repeated indices occurring on the same side of the equation signify summation from 1 to 3 over that index. Thus, each term in Eq. (1) contains 81 terms. This same convention is applied throughout the paper.) Similar bounding relations on the effective elastic compliance tensor are also available [11].

Although Eq. (1) rigorously bound the elastic energy density, bounding of the effective stiffness tensor itself is only convenient when the indices k, l are set equal to i, j. In this situation the following bounds must be satisfied:

$$\begin{aligned}\bar{S}^{-1}_{ijij} \le C^{\text{eff}}_{ijij} \le \bar{C}_{ijij}\\ \bar{C}^{-1}_{ijij} \le S^{\text{eff}}_{ijij} \le \bar{S}_{ijij}\end{aligned} \tag{2}$$

Thus, bounds on 9 of the 21 independent effective elastic constants are readily available from simple volume averages over the corresponding local elastic constants, but more complex relations are required to bound the remaining terms [10,11]. For our purposes in this paper, we will focus upon the *Hill-average elastic constants*, $C^{\text{eff(Hill)}}$ and $S^{\text{eff(Hill)}}$, which are defined by the following expressions:

$$\begin{aligned}C^{\text{eff(Hill)}}_{ijkl} \approx \frac{\bar{S}^{-1}_{ijkl} + \bar{C}_{ijkl}}{2}\\ S^{\text{eff(Hill)}}_{ijkl} \approx \frac{\bar{C}^{-1}_{ijkl} + \bar{S}_{ijkl}}{2}\end{aligned} \tag{3}$$

The Hill-average constants are an average of the upper- and lower-bounds on the effective elastic constants; and the expressions apply to all 21 independent components.

Refinements in the prediction of elastic constants are available [10,11], but such require additional information on the spatial placement of local state, in addition to the distribution by volume fraction. For our purposes the Hill-average estimates will be sufficient.

2.2 Distribution of Local States. The term *local state* refers here to any local characteristic of the material that affects the property of interest. *Local state distribution* refers to how the components of microstructure are distributed upon the set of possible local states. A common example of a local state distribution function is the familiar orientation distribution function, used in describing the crystallographic texture of polycrystals [13]. For the materials of interest in this paper, two types of local state will be important, but only one will be considered to vary. Only one material phase is present in oxygen free electronic (OFE) Cu polycrystals—the FCC Cu phase. Impurity levels in this material are small; and these impurities are typically dispersed in interstitial form within the dominant phase. It is assumed that the local elastic state of the material is determined only by the orientation of the crystal lattice and by the basic elastic properties of the Cu phase, C^{Cu}. If the direction cosines, $g(x)$, are known at any local position x, then the local elastic properties are given by the expression

$$C_{ijkl}(x) = g_{im}(x)g_{jn}(x)g_{ko}(x)g_{lp}(x)C^{Cu}_{mnop} \tag{4}$$

The sense of the direction cosines in this expression is a coordinate transformation from the $\langle 100\rangle$ crystal axes of the FCC unit cell, to the selected orthonormal coordinate system in the macroscopic or specimen frame. Clearly $g(x)$ varies little when x varies within an individual grain, but it jumps as x traverses a grain boundary.

$g(x)$ is the local state variable of principal interest in this paper. With respect to the Hill-average estimates of effective elastic properties, given by Eq. (3). Equation (4) can be used as input into volume averaging, if $g(x)$ is known for a sufficient sampling of material points x. Current experimental electron backscatter diffraction (EBSD) techniques [11,14] are very efficient at measuring $g(x)$ for large numbers of material points.

The second local state variable of interest to the present work is the *critical resolved shear stress*, τ_{CRSS}. This reflects the level of shear stress that must be present upon any of the $\{111\}\langle 110\rangle$ slip systems to cause dislocation slip to occur. It is known that τ_{CRSS} is proportional to the square root of the local total dislocation density, which typically varies with position x. However, in the present work τ_{CRSS} will be held constant for any specified material condition within the database. Determination of τ_{CRSS} will be discussed later.

Various parameterizations of $g(x)$ are available. Of course the full 3×3 matrix of coefficients of the direction cosines, utilized in Eq. (4), is an important parameterization; however only three of the nine direction cosines are independent [11,13]. And for the purposes of defining the range of all possible lattice orientations, it is convenient to reduce $g(x)$ to three independent variables. Many choices are possible, but the Bunge Euler angles, ϕ_1, Φ, ϕ_2, are the most common [13]. These define a sequence of three primitive rotations that are required to bring a sample-fixed coordinate frame into coincidence with the lattice fixed frame on $\langle 100\rangle$. Output of the Bunge Euler angles is common, using established image processing applied to EBSD patterns [14]. When symmetry of the FCC crystal lattice is fully considered, it is convenient to express a threefold redundant space of possibilities for ϕ_1, Φ, ϕ_2 [11]

$$FZ_{3C} = \left\{ g \equiv (\phi_1, \Phi, \phi_2) \middle\| \begin{array}{l} 0 \le \phi_1 < 2\pi \\ 0 \le \Phi < \dfrac{\pi}{2} \\ 0 \le \phi_2 < \dfrac{\pi}{2} \end{array} \right\} \tag{5}$$

The threefold redundancy refers to the fact that each physically distinctive lattice orientation appears 3 times in FZ_{3C}. Further reduction to the point that each distinctive orientation appears only one time is possible, but the inconvenience is that the fundamental zone contains a complex surface, which renders partitioning difficult. Experience dictates that it is easier to work with the

rectangular threefold redundant fundamental zone described by Eq. (5). From the experimental point of view, each EBSD-based measurement of lattice orientation will occur 3 times in FZ_{3C}.

The rectangular shape of FZ_{3C} can be split into smaller bins of regular, rectangular shape. All computations of the type required in Eq. (3) will be handled discretely, using binned datasets. Suppose that N such bins have been defined, and designated by ω_n, where

$$\omega_n \subset FZ_{3C}, \quad \bigcup_{n=1}^{N} \omega_n = FZ_{3C}, \quad \omega_n \cap \omega_m = \oslash \ (m \neq n) \tag{6}$$

Associated with each bin ω_n is an indicator function $\chi_n(g)$, defined by the expression

$$\chi_n(g) \equiv \chi_n(\phi_1, \Phi, \phi_2) \begin{cases} 1, & \text{if } g \in \omega_n \\ 0, & \text{otherwise} \end{cases} \tag{7}$$

The size of the bins will have an effect upon the errors in forming the averages required by the Hill estimates of effective elastic stiffness.

The pertinent local state distribution is the distribution of lattice orientation among the sampled material points. Imagine that a total of S local orientations have been measured by EBSD-based methods. A condition of statistical sufficiency is assumed for this set of measurements. Roughly, this means that the measurements are taken in a sufficiently large number of components of microstructure (grains) to ensure that the experimental sampling is characteristic of the overall microstructure. After converting each of the S measurements of orientation into its three equivalent orientations within FZ_{3C}, the $3S$ determined orientations will be distributed among the N defined bins. Let f^n denote the fraction of $3S$ orientations that fall within ω_n:

$$f^n = \frac{1}{3S} \sum_{s=1}^{3S} \chi_n\{g_s\} \tag{8}$$

The local state distribution function, in this case closely related to the orientation distribution function, will consist in the set of real number fractions $f^n, F = \{f^1, f^2, \ldots, f^N\}$. Clearly, from Eq. (8) conservation of volume requires that

$$\sum_{n=1}^{N} f^n = 1 \tag{9}$$

Approximations to the average elastic tensors required in Eq. (3) are readily formed from the local state distribution function via expressions of the form

$$\bar{C}_{ijkl} \approx \sum_{n=1}^{N} f^n C^n_{ijkl} \tag{10}$$

where C^n denotes the value of the elastic stiffness calculated by Eq. (4) with ϕ_1, Φ, and ϕ_2 taken to be a characteristic lattice orientation lying within the associated bin ω_n. Numerical examination of the bin-size dependency of calculations like Eq. (10) have determined that numerical errors are $\sim 1\%$ when a bin size of $5^\circ \times 5^\circ \times 5^\circ$ in the three Euler angles is selected within FZ_{3C}; consequently, this bin size was utilized throughout the present work.

2.3 Taylor-Bishop-Hill Model. Since its introduction in 1938, the Taylor [6] first-order upper bound on the yield strength of rigid elastic (elastic strains are ignored), perfectly-plastic (strain hardening is not considered) polycrystals [15] has been widely applied to the problem of yielding. Of course these simplified conditions do not accurately reflect the heterogeneous nature of elastic/plastic behavior in polycrystals at the yield point. Essential to the Taylor model is the approximation that all crystallites or grains are subject to the same plastic strain. In the original theory, plastic deformation is constrained to occur by shear on specified slip systems, and the required plastic shear strains on these slip systems are discovered. In FCC materials like Cu, which has 12 $\{111\}\langle 110\rangle$ slip systems, a large number of choices of five slip systems (required to accommodate an arbitrary incompressible plastic deformation) can be discovered from among the 12 available slip systems. At this point Taylor postulates that the correct combination will be the set that accomplishes the required deformation with the least amount of total shear: the so-called minimum work criterion. (Those practiced in the Taylor model will recall that it is often the case that there remains a redundancy in the available sets of slip accommodation. Several choices remain with the same minimum work condition. However, for consideration of yield strength alone, this redundancy is of no further interest.)

The question naturally arose after the emergence of the Taylor model, as to whether or not actual homogeneous stress conditions could be discovered that would activate any particular required set of slip systems for yielding. Thus came the Bishop-Hill model in 1951 [7,8]. It was discovered that for FCC materials a set of 56 stress states are capable of activating the required combinations of slip for an arbitrary plastic deformation. These 56 stress states are also known as *stress corners*, because they form the vertices of a convex polytope, which is the yield surface in 5D deviatoric stress space. A maximum work criterion was presented for correctly identifying the pertinent stress corner associated with any particular impressed plastic strain. Later Chin and Mammel showed that the Taylor and Bishop-Hill models are dual solutions to the same linear problem [16]. For this reason some authors refer to these two complimentary models as the Taylor-Bishop-Hill (TBH) model.

These 56 vertices or corners of the yield surface for FCC crystals can be grouped into five different types: the first three groups activate eight slip systems simultaneously; and the second and third groups activate six slip systems [7,17]. According to the TBH model, a slip system is only activated when the resolved shear stress meets or exceeds τ_{CRSS}. It is also found that the resolved shear stress upon the nonactive slip systems is zero [17]. Appendix B lists 28 of the 56 TBH corner stress states; the remaining 28 are simply related to the first 28 by a minus sign.

According to the TBH model, each grain experiences the uniform (macroscopic) imposed strain. TBH theory hypothesizes that the active corner stress state is the one that maximizes the work done. If the local corner stress is σ^C, and the imposed strain increment is $\delta\epsilon$, then the increment of plastic work, δW^p for any particular choice of stress corner will be

$$\delta W^p = \sigma^C_{ij}(x)\delta\varepsilon_{ij}(x) \tag{11}$$

The correct choice for the active stress corner, within the TBH model, is the one that maximizes δW^p.

First-order estimates of the TBH upper-bound on the yield strength in polycrystals can be computed from the S measurements of lattice orientation, $g(x)$, according to the following expression:

$$\bar{\sigma}^Y_{ij} \approx \sum_{n=1}^{N} f^n \sigma^{Cn}_{ij}(\delta\varepsilon) \tag{12}$$

Here $\delta\epsilon$ is the imposed plastic strain increment, $\bar{\sigma}^Y(\delta\varepsilon)$ is the predicted macroscopic yield stress associated with the selected plastic strain increment, and $\sigma^{Cn}(\delta\epsilon)$ is the correct TBH stress corner associated with bin n and the imposed plastic strain increment, according to Eq. (11). (Note that it is essential that all terms in Eq. (12) be expressed in the macroscopic or specimen coordinate frame.)

2.4 Estimation of τ_{CRSS} from the TBH Model. The corner stress states required to implement the yield stress estimation expressed in Eq. (12) require knowledge of τ_{CRSS}. A particular way of estimating the τ_{CRSS} has been used, and will be briefly described here. It is assumed that experimental uniaxial tensile testing has been conducted on each material of interest.

Tensile samples are cut to a geometry, and loaded in such away that to a first approximation only a single tensile component of the stress can be present in the gage section of the sample. We designate this tensile axis as the $\hat{e}_1$ direction, with the two transverse directions being $\hat{e}_2$ and $\hat{e}_3$. If the tensile testing is conducted with $\hat{e}_1$ aligned with any one of the principal axes of material microstructure, then it is reasonable to expect that the plastic strain increment in the gage section to have a diagonal form that can be expressed as

$$\delta\varepsilon \equiv \delta\varepsilon_{11}\begin{bmatrix} 1 & 0 & 0 \\ 0 & -\eta & 0 \\ 0 & 0 & -(1-\eta) \end{bmatrix} \tag{13}$$

where η is the contractile (plastic) strain ratio, $\eta = \frac{\varepsilon_{22}}{\varepsilon_{11}}$. In principle this contractile strain ratio can be measured in the tensile sample after yielding has occurred, when the load has been removed from the sample. Once the relevant contractile strain ratio is known, the appropriate strain increment is known, and Eq. (12) can be used to estimate the uniaxial yield strength, $\bar{\sigma}^Y_{11}$. This estimate scales linearly with τ_{CRSS}, and adjustments in τ_{CRSS} can be pursued until $\bar{\sigma}^Y_{11}$ matches with the experimentally measured yield stress. This is the basic approach.

In practice it is difficult to measure the plastic contractile strain ratio at initial yielding, because the plastic strains involved are small, $\sim 10^{-3}$. One approach to overcome this is to deform the sample to larger deformations, and then to assume that the contractile strain ratio observed at these larger strains will be representative of the one at smaller strains. The limitations of this approach are obvious. Another approach, which is numerical, is to take the contractile ratio to be a variable, and then to calculate the estimate of the yield stress tensor for each selected choice of the ratio. When the predicted stress state is as close as possible to the uniaxial condition, it can be assumed that the correct contractile ratio has been discovered. This approach is equivalent to minimizing the average overall plastic work increment, δW^p. In the present work, this latter approach has been taken.

2.5 Determination of Elastic-Yield Property Closures. Interest in the complete range of elastic/yield property combinations that could occur within all conceivable polycrystalline microstructures of fixed material phase typically occurs during preliminary design. Theoretical methods for constructing estimates of properties closures have been presented in the literature [11,18–20]. The approach taken is to make use of available microstructure-sensitive homogenization relations for the properties of interest, and then to consider all possible microstructures, beginning with single crystals of an arbitrary lattice orientation. Details of this approach are not given here; but the interested reader will find the methods detailed in the referenced literature [11,18–20]. Of interest in this paper is a limited, or *accessible properties closure*, comprising the portion of the full elastic/yield closure that is readily accessible with ordinary materials processing.

2.6 Anisotropic Properties of Orthotropic Plates Containing Circular Holes. As an example of a simple anisotropic design problem, where microstructure considerations are of paramount importance, the classical problem of *a hole in an anisotropic plate* will be revisited. The detailed mechanics of plates containing a circular hole, and with microstructures exhibiting orthorhombic symmetry, was presented by Lekhnitskii [12]. Considering an infinite plate, loaded under uniaxial in-plane tension in an arbitrary direction with respect to a selected principal axis of material orthorhombicity, the tensile stress tangential to the inner surface of the hole is given by the expression:

$$\begin{aligned} \sigma_\theta = p\frac{E_\theta}{E_1}\{&[-\cos^2\phi + (k+n)\sin^2\phi]k\cos^2\theta \\ &+ [(1+n)\cos^2\phi - k\sin^2\phi]\sin^2\theta \\ &- n(1+k+n)\sin\phi\cos\phi\sin\theta\cos\theta\} \end{aligned} \tag{14}$$

In this expression p is the applied stress, exerted a large distance away from the circular hole. θ defines an angle relative to the selected principal material axis (taken to be the rolling direction in this work) that identifies the location of a point on the circumference of the circular hole. This is defined to be the tensile stress tangential to the point of circumference identified by θ. Finally, ϕ denotes the direction of the applied stress with respect to the principal material axis. Other components in Eq. (14) are defined by the expressions

$$\begin{aligned} \frac{1}{E_\theta} &= \frac{\sin^4\theta}{E_1} + \left(\frac{1}{G} - \frac{2\nu_1}{E_1}\right)\sin^2\theta\cos^2\theta + \frac{\cos^4\theta}{E_2} \\ k &= \sqrt{\frac{E_1}{E_2}} \\ n &= \sqrt{2\frac{E_1}{E_2} - \nu_1 + \frac{E_1}{G}} \end{aligned} \tag{15}$$

The symbol ν_1 represents Poisson's ratio perpendicular to the principal material axis, E_1 and E_2 represent Young's modulus in the rolling and transverse directions of the sheet, respectively, and G is the in-plane shear modulus. Given the traction-free condition at the circumference of the hole, and the other geometrical and boundary conditions, σ_θ is the only nonzero component of stress that can occur adjacent to the circular hole. Estimates for each of these effective elastic properties are accessible by calculations of the Hill average properties, using Eqs. (3) and (10).

Predictions of σ_θ, taken from Eq. (14), will be compared to estimates of the yield strength, which also varies with θ, in order to establish the maximum value of the tensile load p that can applied to the plate without causing yielding. The design problem reduces to the matter of determining, for any particular material, the peak load that can be applied and the direction ϕ in which it must be applied. Figure 1 depicts the essential geometrical definitions for the anisotropic hole-in-the-plate problem.

3 Proposed Hybrid Bishop-Hill Model

In most yield limited design problems the interest is in the near-vicinity of the yield surface, where the plastic strain is not dominant compared with the elastic strain. If the spatial character of the strain state is considered, it is not constant, but varies with position in complex ways. These conditions call to question the

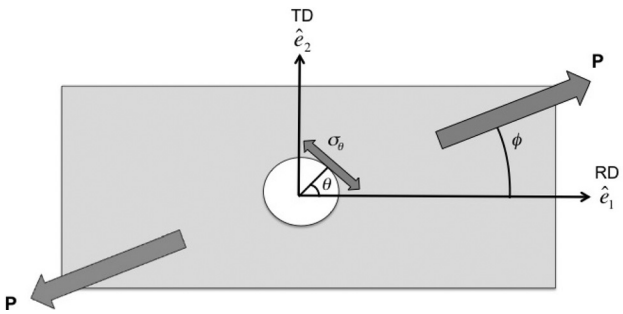

Fig. 1 A geometry of anisotropic hole-in-plate problem

Table 1 Sample description

Sample description	Heat treatment temperature (°C)	Heat treatment time (Hour)
As received	N/A	N/A
As received and annealed	191	1
98% cold worked	N/A	N/A
98% cold worked and recrystallized	225	0.5
58% cold worked	N/A	N/A
58% cold worked and annealed	160	1
58% cold worked and recrystallized	225	1.5
Cube texture	N/A	N/A

application of the TBH model for the problem of initial yielding. For plastic problems where the total strain is dominated by the plastic component, this is not an issue.

Our present purpose is to propose a modified version of the TBH model, which will be named the *Hybrid Bishop-Hill Model* (HBH model). Importantly, the focus of the HBH model is on the applied stress, rather than on the plastic strain; this makes the model much more accessible to design engineers who focus more upon stress states, rather than strain states. The algorithm for predicting the yield strength of the polycrystalline material via the HBH model uses the same stress corners that were defined for the TBH model. Retaining this characteristic means that there will be a natural heterogeneity of local stress among the constituents of the polycrystal.

A simple assumption is taken that the local yielding at any position in the material occurs at that corner stress state, $\hat{\sigma}^C_{ij}$, that lies "closest" to the macroscopic stress, $\hat{\sigma}_{ij}$. The "hat" over the stress symbols signifies the deviatoric stress. Distance between these two stress states is defined by d_{ij}, where

$$d_{ij} = \hat{\sigma}^c_{ij} - \hat{\sigma}_{ij} \tag{16}$$

The magnitude of distance between stress states, d, is defined by the Euclidean norm

$$||d^2|| = d_{ij}d_{ij} \tag{17}$$

Importantly, the distance defined according to Eqs. (16) and (17) is invariant with respect to coordinate transformation. The selection of stress corner for any particular component (grain) within the polycrystal is taken to be the Bishop-Hill corner stress that minimizes the distance d between the applied stress and the corner stress state.

The estimated (deviatoric) yield strength of the material is obtained from the expression

$$\hat{\sigma}^Y_{ij} \approx \sum_{n=1}^{N} f^n \hat{\sigma}^{Cn}_{ij} \tag{18}$$

$\hat{\sigma}^{Cn}$ denotes the pertinent stress corner associated with bin n in FZ_{3C}. Note that all corner stress states exercised in Eq. (18) must be expressed in the macroscopic (sample) frame in order to interpret $\hat{\sigma}^Y_{ij}$ as the yield strength. Whereas yield strength is customarily described as the full Cauchy stress, the deviatoric yield stress must be converted, using the customary definition

$$\sigma^Y_{ij} = \hat{\sigma}^Y_{ij} + \frac{1}{3}\delta_{ij}\sigma^Y_{kk} \quad \text{(summation over } k \text{ implied)} \tag{19}$$

Exercising Eq. (20) to obtain σ^Y_{ij} requires additional physical information about the applicable pressure $\frac{1}{3}\delta_{ij}\sigma^Y_{kk}$ or some other characteristic of the normal components of σ^Y_{ij} If, for example, the calculations involve estimates of a uniaxial tensile test, then only one component of σ^Y_{ij} is expected to be nonzero; and in this case a pressure term $\frac{1}{3}\delta_{ij}\sigma^Y_{kk}$ can be applied that renders σ^Y_{ij} as close as possible to a uniaxial stress condition. This is the approach taken in the present work.

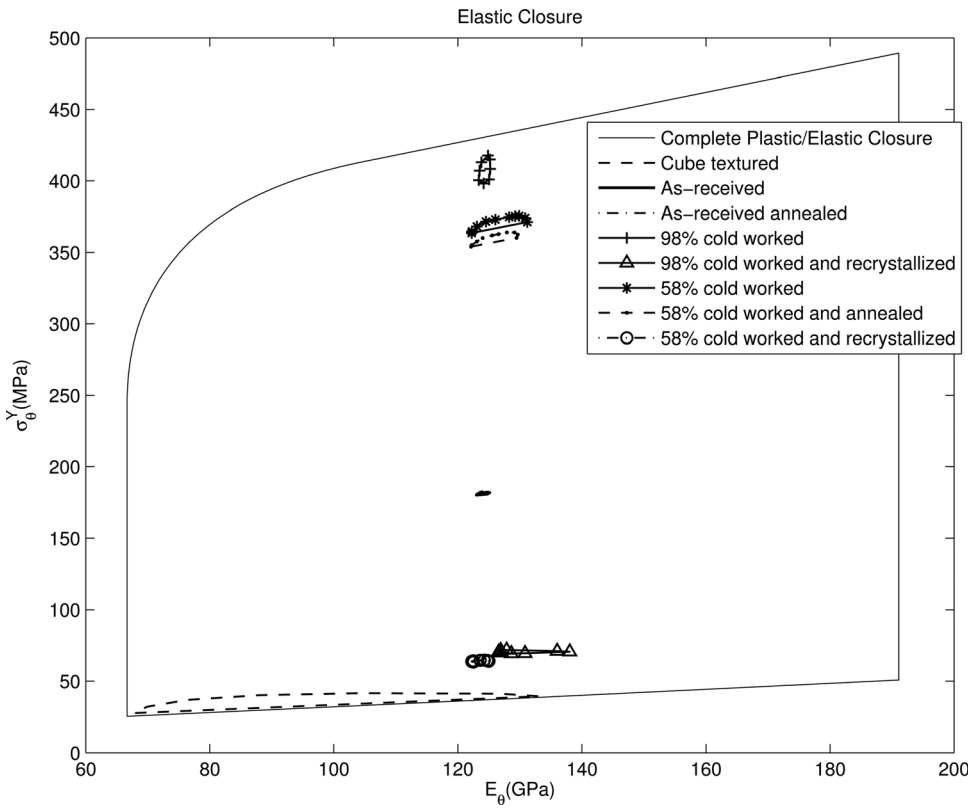

Fig. 2 Property Closure

Table 2 Comparison of experimentally obtained tensile yield strength vs the numerically obtained yield strength

Samples	Contractile strain ratio (H)	Experimental tensile yield strength (MPa)	The TBH yield strength (MPa)	The HBH yield strength (MPa)
As received	0.51	185.40	201.74	181.07
As received and annealed	0.49	185.67	204.05	182.10
98% cold worked	0.43	423.48	436.15	400.95
98% cold worked and recrystallized	0.52	71.93	77.83	69.67
58% cold worked	0.36	377.10	401.11	363.53
58% cold worked and annealed	0.39	363.93	391.08	354.06
58% cold worked recrystallized	0.54	65.43	72.14	63.97
Cube texture	0.39	33.76	50.56	27.65

Recall that the corner stress states of the TBH model are states that are capable of supporting general local states of plastic strain. Consistent with the classical Taylor model, the TBH model defines stresses that are capable of causing an arbitrary plastic strain state, by $\{111\}\langle 110\rangle$ dislocation slip. The TBH model does not satisfy the stress equilibrium condition, although when the macroscopic plastic strain is imposed upon each individual grain within the material, strain compatibility is fulfilled in a trivial sense. The new HBH model fulfills neither stress equilibrium, nor strain compatibility at a local level. However, having utilized the TBH stress corners in the model to estimate local stress conditions, it can be anticipated that complex plastic strain conditions, as required by the equilibrium and compatibility requirements under elastic/plastic loading, could more readily be satisfied by

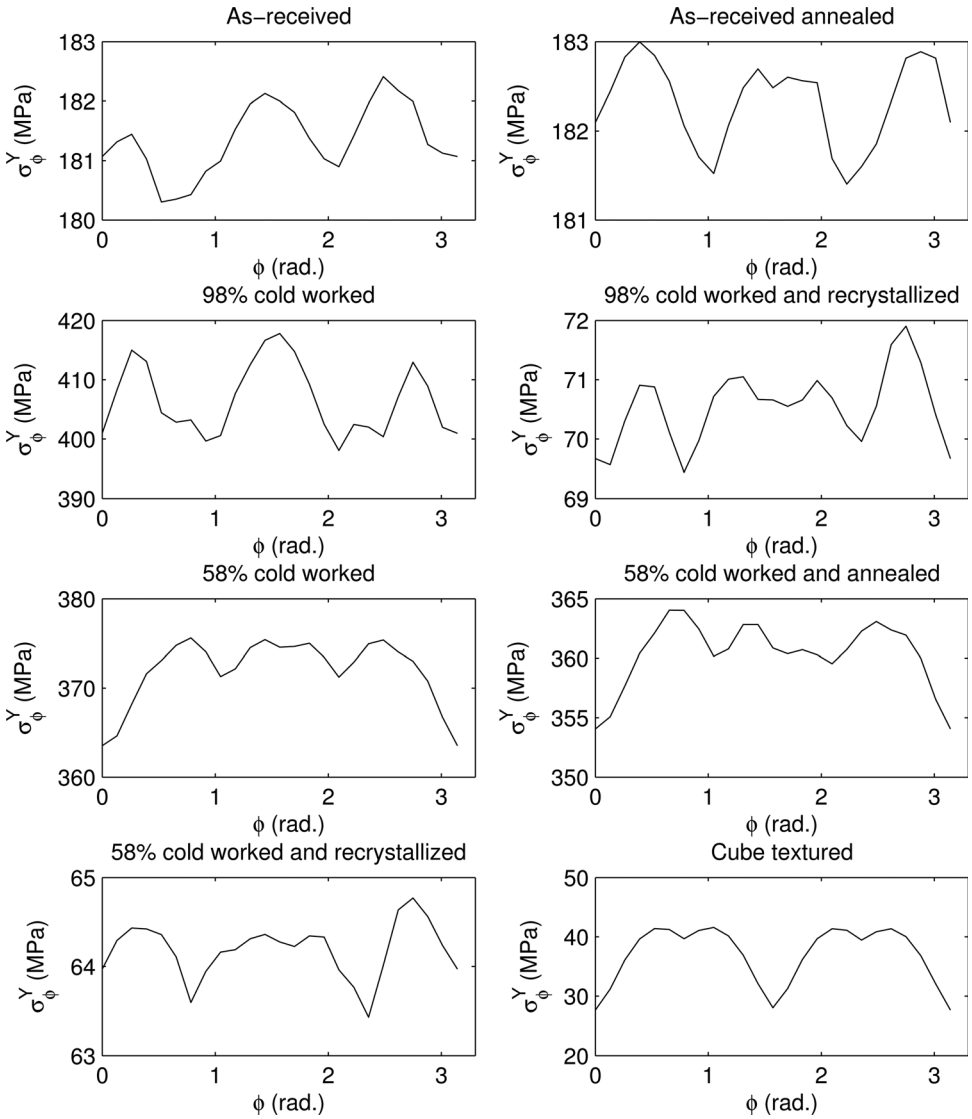

Fig. 3 A variation in yield strength with respect to the applied tensile load direction in anisotropic plates

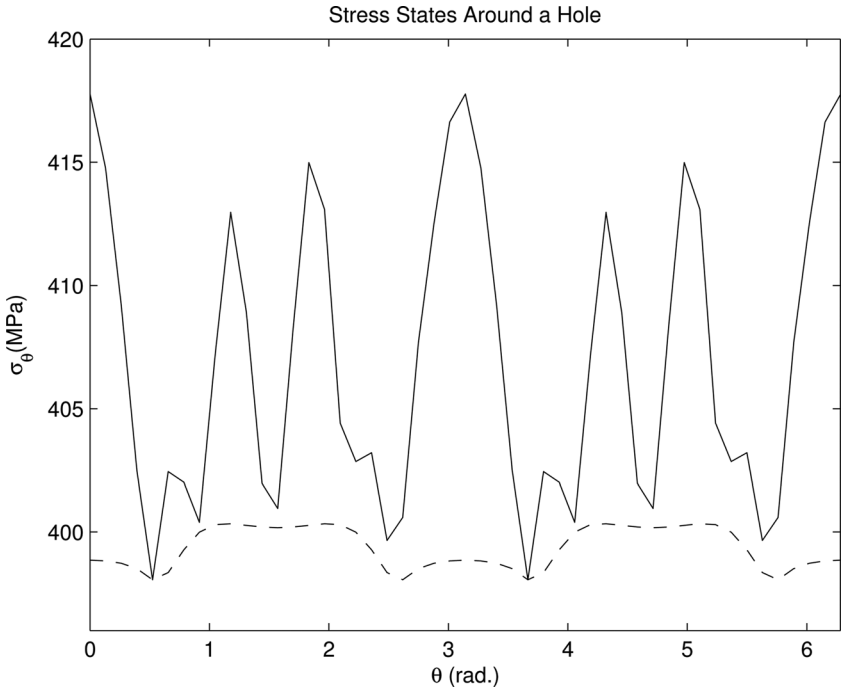

Fig. 4 The stress states around a circular hole in 98% cold worked plate. The solid line indicates the yield surface of the material, and the dotted line indicates the stress states around the hole. When the stress states (σ_θ) touch the yield surface (σ_θ^Y), the material is considered to be yield. The applied stress is along the sample rolling direction.

the stress corners. To some extent the HBH model could be compared to the relaxed-constraints model(s) that preserve some features of Taylor-like models, but do not strictly enforce either strain compatibility or stress equilibrium [21].

The basic relations pertaining to the HBH model (Eqs.(16)–(18)) can be applied to arbitrarily complex loading states.

4 Results and Discussions

4.1 Database of OFE Copper Materials. It will be obvious to those familiar with materials processing, that the range of microstructures that are readily accessible to the designer comprise a range of properties that is much smaller than the set considered by the theoretical properties closure, briefly described in Sec. 2.5 above. A limited, accessible closure for elastic/yield properties has been considered for OFE Cu. Three common processing routes have been considered: rolling deformation, thermal annealing, and rigid body rotation of the material about the normal direction to the rolling plane. Rolled OFE Cu plate (in the as-received "half-hard" condition), and six derivative materials produced there-from by secondary processing steps, and one addition material (very strongly "cube textured," provided by Oak Ridge National Laboratory), were considered in the database. Table 1 describes the processing conditions for each of these samples.

Theoretically, each of these eight materials within the "accessible" database, were then allowed to rotate around their plane normal, in order to compute the *accessible properties closure*. The local state distribution can easily be recomputed for an arbitrary rotation angle, and then Eqs. (10) and (12) can be reexercised to recover the changed estimates for elastic and yielding properties. Rotations of the sample relative to the loading gives rise to orbits in the properties closure. Further details of this approach are provided in the 2008 paper of Adams et al. [18]. The complete and accessible closure for σ_θ^Y (in-plane uniaxial yield strength in direction $\hat{\theta}$) versus E_θ (Young's modulus associated with the same in-plane direction) is shown in Fig. 2. The reader should note that E_1 in Eqs. (14) and (15) is related to this notation by $E_1 = E_0 = E_{\theta=0}$ and $E_2 = E_{\pi/2} = E_{\theta=\pi/2}$.

4.2 Comparison of HBH and TBH Models. An accessible comparison is here detailed for the predictions of yield strength for the eight OFE Cu materials included in the database of this study. The comparison is between predictions based upon the classical TBH and the new HBH models.

Appendix A contains the {111} and {200} crystallographic pole figures for each material of the database. These were obtained from EBSD data sets comprising a minimum of 2500 grains for each sample (excluding the "cube textured" material, which has a large grain size). The peak value for the texture of these materials was measured to be in excess of 37 "times-random," for the cube-textured, sample, for the $\{100\}\langle 001\rangle$ component. Most of the other materials exhibited the classical rolling texture, [22] with peak times-random values ranging from 1.6 in the as-received material, upwards to 5.5 in the 98% cold worked sample. It is evident that upon annealing the 98% cold rolled material, a $\{100\}\langle 001\rangle$ cube component develops with an intensity of ~ 3.7 times random.

Standard tensile testing was conducted for the purpose of recovering the yield strength in the rolling direction, RD, in each sample. (The yield strengths reported are the typically average values from three tensile tests.) Using the numerical approach described in Sec. 2.4 above, the contractile strain ratio η was varied in connection with Eqs. (11) and (12) until the macroscopic increment of plastic work, $\delta\bar{W}^p$, estimated from the TBH model, was minimized. Using this estimate for the strain increment, τ_{CRSS} was estimated from the Taylor factor, the yield strength, estimated from the TBH model, was recorded. This was compared with the yield strengths predicted for the same materials using the HBH model, by taking the applied stress to be a uniaxial tensile stress in RD. The results of this comparison are shown in Table 2. It is evident that in most instances the new HBH model more accurately predicts the yield strength in comparison with the TBH model.

4.3 HBH-Based Design for the Anisotropic Hole-In-The-Plate Problem. First, consider the plate without a hole. Variation of the uniaxial yield strength, σ_ϕ^Y with direction of the applied load, ϕ, is shown in Fig. 3 for each of the eight materials within the database. The natural variation of yield strength is as small as ~1% in the as-received and as-received annealed materials, to ~33% in the strongly cube-textured material. In terms of absolute strength, it is not unexpected that the lowest values of strength are found in the most heavily annealed materials, and the highest values are seen in the most heavily cold-worked material. The range of strength is from ~ 30 to 425 MPa.

Next, consider plates containing a circular hole, loaded under uniaxial tension. The simple stress states around the circumference of the hole, are purely uniaxial; and they act in a tangential direction relative to the circumference of the hole. This is expressed by Eqs. (14) and (15). This stress state can be compared with the theoretical yield stress in the same direction, as determined using the HBH model. Note that σ_θ depends linearly upon the magnitude of the stress p applied in direction ϕ; and the magnitude of σ_θ depends on both variables, ϕ and θ. In this paper, we have taken the liberty of describing two kinds of uniaxial stress, σ_ϕ and σ_θ. In the first case σ_ϕ denotes a uniaxial stress aligned with the direction defined by ϕ; and with respect to the hole-in-the-plate problem, $\sigma_\phi = p$. σ_θ, however, in the context of the hole-in-the-plate problem, is the tangential stress acting at the point identified by θ on the circumference of the circular hole, as shown in Fig. 1, evidenced by Eqs. (14) and (15), $\sigma_\theta = \sigma_\theta(p,\phi)$. The distinction between σ_ϕ and σ_θ is that the former is parallel to the direction defined by ϕ, and the latter is perpendicular to the direction specified by θ. When the superscript Y is used, as with σ_ϕ^Y or σ_θ^Y what is meant is the uniaxial yield strength of the material in the same sense as the stress state.

Figure 4 compares the θ—dependent yield strength, σ_θ^Y versus the stress state around the circumference of the circular hole for the 98% cold-worked OFE Cu plate. For this example ϕ was chosen to be 0 (i.e., along RD), and the magnitude of the applied stress, p, was taken at a level that just causes these two curves to touch one another at $\theta = 30$ and 210 deg, at a stress level of 398 MPa. For stress levels that exceed this it is predicted that plastic yield will occur, first at these two circumferential angles, and then later at other locations associated with minima in the yield strength curve. Note that changes in the angle ϕ of application of the applied stress p will change the form of σ_θ. Peak performance in design with plates containing circular holes will consist in

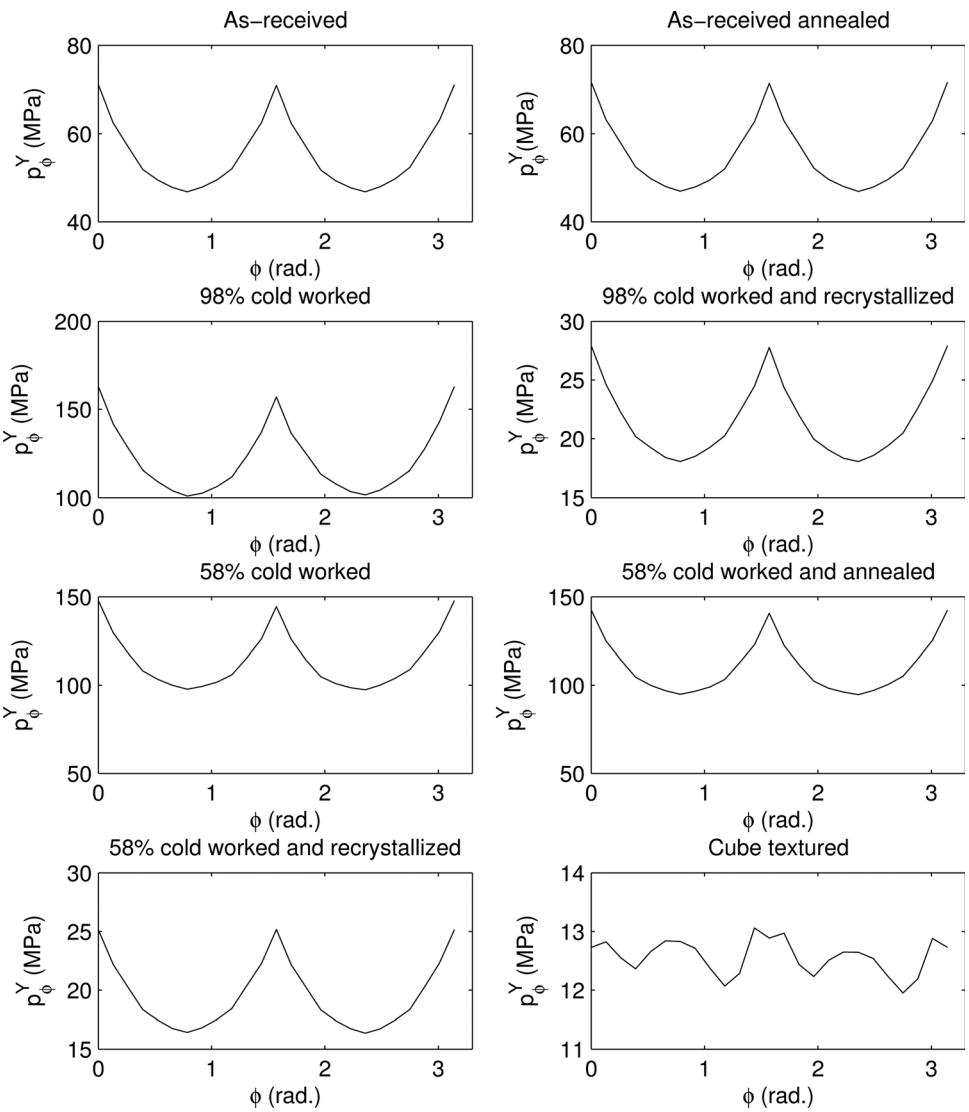

Fig. 5 A variation in yield strength with respect to the applied tensile load direction in anisotropic plates with a circular hole

Table 3 The performance of anisotropic plates with a circular hole

Samples	Performance	Stress concentration (K_t)	Applied tensile yield strength (p_ϕ^Y) (MPa)	Angles from the sample rolling direction (degrees)
As received	Max	2.54	71.05	0, 90
	Min	3.86	46.80	45, 135
As received and annealed	Max	2.54	71.58	0, 90
	Min	3.87	46.90	45, 135
98% cold worked	Max	2.44	162.99	0, 90
	Min	3.96	100.89	45, 135
98% cold worked and recrystallized	Max	2.49	27.91	0, 90
	Min	3.88	18.04	45, 135
58% cold worked	Max	2.46	147.82	0, 90
	Min	3.73	97.40	45, 135
58% cold worked and annealed	Max	2.49	142.37	0, 90
	Min	3.74	94.64	45, 135
58% cold worked recrystallized	Max	2.54	25.17	0, 90
	Min	3.88	16.36	45, 135
Cube texture	Max	2.15	13.06	82.5
	Min	2.31	11.95	157.5

identifying the direction ϕ at which the largest p can be applied without causing plastic yielding at any position θ about the hole.

This same analysis can be performed for all of the plate types found in the database, and the peak value of p, at each direction ϕ in the plate, at which yielding first occurs, can be identified. Let p_ϕ^Y denote the applied load in direction ϕ where yielding begins. This behavior is shown in Fig. 5.

Likewise the minimum performance can also be obtained using the same approach, but noting the lowest performance. This minimum performance is interesting from the point of view that an uninformed designer could inadvertently load a plate with circular hole in the direction where minimum strength would be realized. Another way to look at the maximum and minimum performance is in terms of the associated stress concentration factors. An anisotropic stress concentration factor, K_t can be defined as the following:

$$K_t = \frac{\max \sigma_\theta}{p_\phi^Y} \tag{20}$$

where max σ_θ signifies the peak value of σ_θ that occurs around the circumference of the hole at the applied load at which yielding occurs, p_ϕ^Y. For isotropic materials K_t becomes 3, but for anisotropic materials it can be larger or smaller than 3. A complete listing of the predicted maximum and minimum performance levels, their associated yield strengths p_ϕ^Y and the angles of load application, and their related stress concentration factors, is presented in Table 3.

The reader will note that a wide range of K_t is associated with the predicted maximum and minimum performance conditions among the materials of the database. The predicted range is $2.15 < Kt < 3.96$, or nearly a factor of 2.

5 Conclusion

This paper presents a new approach to first-order yield limited elastic/plastic design, by introducing the Hybrid Bishop-Hill model for yielding. The HBH model retains the distinctive corner stress states defined for FCC crystals by the classical Taylor Bishop-Hill model, but differs in focusing the choice of corner stress state upon the macroscopic applied stress. In a comparison between the TBH and HBH models, undertaken for a database of eight distinctive OFE Cu materials, it was demonstrated that the HBH model performed markedly better than the TBH model when compared with experimentally measured yield strengths. A complete properties closure for in-plane uniaxial yield strength versus Young's modulus was presented, and compared with an accessible property closure for the database of eight OFE Cu materials. In addition to the varied secondary processing by thermal-mechanical treatment, rigid body rotation of these sheet materials, about the sheet normal, was considered. The variation of yield strength and Young's modulus with rotation define orbits within the properties closure. These orbits were detailed in the accessible property closure. In order to illustrate the application of the new HBH model to a yield limited design problem of general interest, the problem of yielding in anisotropic plates containing circular holes was considered. Anisotropic plate theory predicts that the location of stress concentration is dependent on material microstructure such that the stress concentration is not necessary located at 90 deg off the applied tensile load axis, as in the isotropic plate theory, but varies with material microstructure and loading direction in the plate. By identifying the optimal (and critical) directions of the applied tensile load, the designer can improve the performance of plates as much as 62%. In the identified optimal direction it is predicted that the applied stress at yield is about 40% of the tensile yield strength in the rolling direction, except for the cube-textured material; the minimum performance, associated with the critical direction, is typically about 25% of the tensile strength. The cube textured plate shows a unique quality among the samples studied in this paper. Both the optimal and critical performance of plate with a circular hole is about 40% of the yield strength in the nonperforated plate. The difference in yield strength between the optimal and critical directions is the smallest in cube textured anisotropic plates containing a circular hole; i.e., the material exhibits a weak directional dependence on applied load direction. This paper has presented a new approach to improve the performance of simple mechanical parts by incorporating material microstructure information into a stress-centric framework. Since the stress is much more accessible than the plastic strain, near the yield point of the material, the new approach facilitates a much easier approach to yield limited design. As an example of the application of the new yield theory, we have shown that the locations of stress concentration, the optimal/critical applied load directions, and the readily accessible direction-dependent yield strength predictions aid the design for improvement of overall performance of plates containing a circular hole.

Acknowledgment

This research was funded by the U.S. National Science Foundation, through Grant No. CMMI-0800904. The authors would also like to thank Dr. Amit Goyal of Oak Ridge National Laboratory for providing the cube-textured copper samples.

Appendix A: Pole Figures for the Database

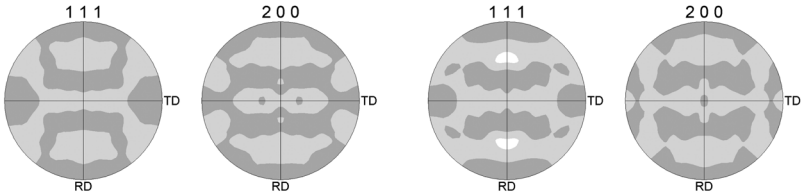

(a) As-received. Maximum intensity: 1.639×random

(b) As-received and annealed. Maximum intensity: 1.748×random

Fig. 6 (*a*) As-received. Maximum intensity: 1.639 × random and (*b*) as-received and annealed. Maximum intensity: 1.748 × random.

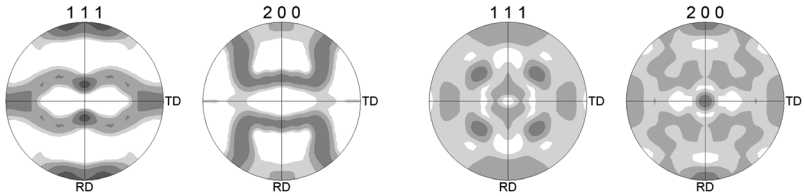

(a) 98% cold worked. Maximum intensity: 5.534×random

(b) 98% cold worked and recrystallized. Maximum intensity: 3.714×random

Fig. 7 98% cold worked. Maximum intensity: 5.534 × random and (*b*) 98% cold worked and recrystallized. Maximum intensity: 3.714 × random.

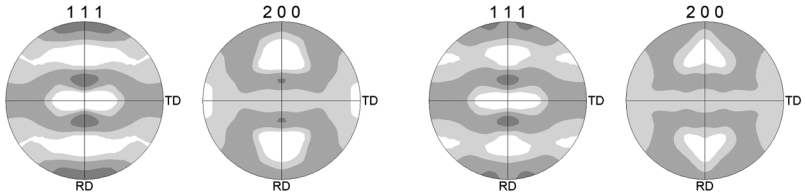

(a) 58% cold worked. Maximum intensity: 3.390×random

(b) 58% cold worked and annealed. Maximum intensity: 2.827×random

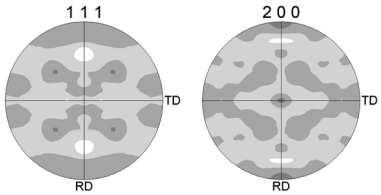

(c) 58% cold worked and recrystallized. Maximum intensity: 2.816×random

Fig. 8 (*a*) 58% cold worked. Maximum intensity: 3.390 × random, (*b*) 58% cold worked and annealed. Maximum intensity: 2.827 × random, and (*c*) 58% cold worked and recrystallized. Maximum intensity: 2.816 × random.

Appendix B: TBH Corner Stress States

Table 4 TBH corner stress states

	σ_{11}^c	Σ_{22}^c	σ_{33}^c	σ_{23}^c	σ_{13}^c	σ_{12}^c
Corner 1	$\sqrt{6}\tau_{\mathrm{CRSS}}$	$-\sqrt{6}\tau_{\mathrm{CRSS}}$	0	0	0	0
Corner 2	0	$\sqrt{6}\tau_{crss}$	$-\sqrt{6}\tau_{\mathrm{CRSS}}$	0	0	0
Corner 3	$-\sqrt{6}\tau_{\mathrm{CRSS}}$	0	$\sqrt{6}\tau_{\mathrm{CRSS}}$	0	0	0
Corner 4	0	0	0	$\sqrt{6}\tau_{\mathrm{CRSS}}$	0	0
Corner 5	0	0	0	0	$\sqrt{6}\tau_{\mathrm{CRSS}}$	0
Corner 6	0	0	0	0	0	$\sqrt{6}\tau_{\mathrm{CRSS}}$
Corner 7	$\frac{\sqrt{6}}{2}\tau_{\mathrm{CRSS}}$	$-\sqrt{6}\tau_{\mathrm{CRSS}}$	$\frac{\sqrt{6}}{2}\tau_{\mathrm{CRSS}}$	0	$\frac{\sqrt{6}}{2}\tau_{\mathrm{CRSS}}$	0
Corner 8	$\frac{\sqrt{6}}{2}\tau_{\mathrm{CRSS}}$	$-\sqrt{6}\tau_{\mathrm{CRSS}}$	$\frac{\sqrt{6}}{2}\tau_{\mathrm{CRSS}}$	0	$-\frac{\sqrt{6}}{2}\tau_{\mathrm{CRSS}}$	0
Corner 9	$-\sqrt{6}\tau_{\mathrm{CRSS}}$	$\frac{\sqrt{6}}{2}\tau_{\mathrm{CRSS}}$	$\frac{\sqrt{6}}{2}\tau_{\mathrm{CRSS}}$	$\frac{\sqrt{6}}{2}\tau_{\mathrm{CRSS}}$	0	0
Corner 10	$-\sqrt{6}\tau_{\mathrm{CRSS}}$	$\frac{\sqrt{6}}{2}\tau_{\mathrm{CRSS}}$	$\frac{\sqrt{6}}{2}\tau_{\mathrm{CRSS}}$	$-\frac{\sqrt{6}}{2}\tau_{\mathrm{CRSS}}$	0	0
Corner 11	$\frac{\sqrt{6}}{2}\tau_{\mathrm{CRSS}}$	$\frac{\sqrt{6}}{2}\tau_{\mathrm{CRSS}}$	$-\sqrt{6}\tau_{\mathrm{CRSS}}$	0	0	$\frac{\sqrt{6}}{2}\tau_{\mathrm{CRSS}}$
Corner 12	$\frac{\sqrt{6}}{2}\tau_{\mathrm{CRSS}}$	$\frac{\sqrt{6}}{2}\tau_{\mathrm{CRSS}}$	$-\sqrt{6}\tau_{\mathrm{CRSS}}$	0	0	$-\frac{\sqrt{6}}{2}\tau_{\mathrm{CRSS}}$
Corner 13	$\frac{\sqrt{6}}{2}\tau_{\mathrm{CRSS}}$	0	$-\frac{\sqrt{6}}{2}\tau_{\mathrm{CRSS}}$	$\frac{\sqrt{6}}{2}\tau_{\mathrm{CRSS}}$	0	$\frac{\sqrt{6}}{2}\tau_{\mathrm{CRSS}}$
Corner 14	$\frac{\sqrt{6}}{2}\tau_{\mathrm{CRSS}}$	0	$-\frac{\sqrt{6}}{2}\tau_{\mathrm{CRSS}}$	$-\frac{\sqrt{6}}{2}\tau_{\mathrm{CRSS}}$	0	$\frac{\sqrt{6}}{2}\tau_{\mathrm{CRSS}}$
Corner 15	$\frac{\sqrt{6}}{2}\tau_{\mathrm{CRSS}}$	0	$-\frac{\sqrt{6}}{2}\tau_{\mathrm{CRSS}}$	$\frac{\sqrt{6}}{2}\tau_{\mathrm{CRSS}}$	0	$-\frac{\sqrt{6}}{2}\tau_{\mathrm{CRSS}}$
Corner 16	$\frac{\sqrt{6}}{2}\tau_{\mathrm{CRSS}}$	0	$-\frac{\sqrt{6}}{2}\tau_{\mathrm{CRSS}}$	$-\frac{\sqrt{6}}{2}\tau_{\mathrm{CRSS}}$	0	$-\frac{\sqrt{6}}{2}\tau_{\mathrm{CRSS}}$
Corner 17	0	$-\frac{\sqrt{6}}{2}\tau_{\mathrm{CRSS}}$	$\frac{\sqrt{6}}{2}\tau_{\mathrm{CRSS}}$	0	$\frac{\sqrt{6}}{2}\tau_{\mathrm{CRSS}}$	$\frac{\sqrt{6}}{2}\tau_{\mathrm{CRSS}}$
Corner 18	0	$-\frac{\sqrt{6}}{2}\tau_{\mathrm{CRSS}}$	$\frac{\sqrt{6}}{2}\tau_{\mathrm{CRSS}}$	0	$-\frac{\sqrt{6}}{2}\tau_{\mathrm{CRSS}}$	$\frac{\sqrt{6}}{2}\tau_{\mathrm{CRSS}}$
Corner 19	0	$-\frac{\sqrt{6}}{2}\tau_{\mathrm{CRSS}}$	$-\frac{\sqrt{6}}{2}\tau_{\mathrm{CRSS}}$	0	$\frac{\sqrt{6}}{2}\tau_{\mathrm{CRSS}}$	$-\frac{\sqrt{6}}{2}\tau_{\mathrm{CRSS}}$
Corner 20	0	$-\frac{\sqrt{6}}{2}\tau_{\mathrm{CRSS}}$	$-\frac{\sqrt{6}}{2}\tau_{\mathrm{CRSS}}$	0	$-\frac{\sqrt{6}}{2}\tau_{\mathrm{CRSS}}$	$-\frac{\sqrt{6}}{2}\tau_{\mathrm{CRSS}}$
Corner 21	$-\frac{\sqrt{6}}{2}\tau_{\mathrm{CRSS}}$	$\frac{\sqrt{6}}{2}\tau_{\mathrm{CRSS}}$	0	$\frac{\sqrt{6}}{2}\tau_{\mathrm{CRSS}}$	$\frac{\sqrt{6}}{2}\tau_{\mathrm{CRSS}}$	0
Corner 22	$-\frac{\sqrt{6}}{2}\tau_{\mathrm{CRSS}}$	$\frac{\sqrt{6}}{2}\tau_{\mathrm{CRSS}}$	0	$-\frac{\sqrt{6}}{2}\tau_{\mathrm{CRSS}}$	$\frac{\sqrt{6}}{2}\tau_{\mathrm{CRSS}}$	0
Corner 23	$-\frac{\sqrt{6}}{2}\tau_{\mathrm{CRSS}}$	$\frac{\sqrt{6}}{2}\tau_{\mathrm{CRSS}}$	0	$\frac{\sqrt{6}}{2}\tau_{\mathrm{CRSS}}$	$-\frac{\sqrt{6}}{2}\tau_{\mathrm{CRSS}}$	0
Corner 24	$-\frac{\sqrt{6}}{2}\tau_{\mathrm{CRSS}}$	$\frac{\sqrt{6}}{2}\tau_{\mathrm{CRSS}}$	0	$-\frac{\sqrt{6}}{2}\tau_{\mathrm{CRSS}}$	$-\frac{\sqrt{6}}{2}\tau_{\mathrm{CRSS}}$	0
Corner 25	0	0	0	$\frac{\sqrt{6}}{2}\tau_{\mathrm{CRSS}}$	$\frac{\sqrt{6}}{2}\tau_{\mathrm{CRSS}}$	$-\frac{\sqrt{6}}{2}\tau_{\mathrm{CRSS}}$
Corner 26	0	0	0	$\frac{\sqrt{6}}{2}\tau_{\mathrm{CRSS}}$	$-\frac{\sqrt{6}}{2}\tau_{\mathrm{CRSS}}$	$\frac{\sqrt{6}}{2}\tau_{\mathrm{CRSS}}$
Corner 27	0	0	0	$-\frac{\sqrt{6}}{2}\tau_{\mathrm{CRSS}}$	$\frac{\sqrt{6}}{2}\tau_{\mathrm{CRSS}}$	$\frac{\sqrt{6}}{2}\tau_{\mathrm{CRSS}}$
Corner 28	0	0	0	$\frac{\sqrt{6}}{2}\tau_{\mathrm{CRSS}}$	$\frac{\sqrt{6}}{2}\tau_{\mathrm{CRSS}}$	$\frac{\sqrt{6}}{2}\tau_{\mathrm{CRSS}}$

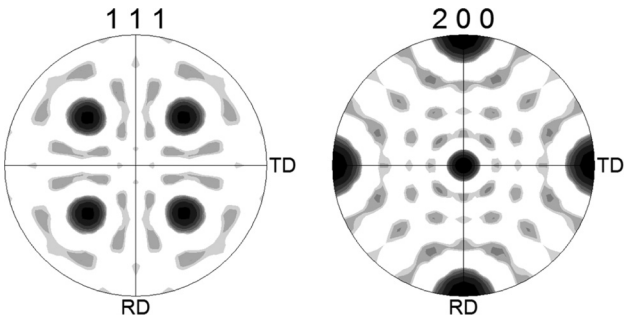

Fig. 9 Cube texture. Maximum intensity: 36.796 × random

References

[1] Ashby, M. F., 2005, *Materials Selection in Mechanical Design*, 3rd., Butterworth-Heinemann, San Francisco.

[2] Juvinall, R. C., 1967, *Engineering Considerations of Stress, Strain, and Strength*, McGraw-Hill, New York.

[3] Canova, G. R., Kocks, U. F., Tome, C. N., and Jonas, J. J., 1985, "The Yield Surface of Textured Polycrystals," J. Mech. Phys. Solids, **33**(4), pp. 371–397.

[4] Lequeu, P., Gilormini, P., Montheillet, F., Bacroix, B., and Jonas, J. J., 1987, "Yield Surfaces for Textured Polycrystals—II. Analytical Approach," Acta Metall., **35**(5), pp. 1159–1174.

[5] Hill, R., 1948, "A Theory of the Yielding and Plastic Flow of Anisotropic Metals," Proc. R. Soc. London, **193** (1033), pp. 281–297.

[6] Taylor, G. I., 1938, "Plastic Strain in Metals," J. Inst. Met., **62**, pp. 307–324.

[7] and Bishop, J. F. W. and Hill, R., 1951, "A Theoretical Derivation of the Plastic Properties of a Polycrystalline Face-Centered Metal," Philos. Mag., **42**, pp. 1298–1307.

[8] Bishop, J. F. W., and Hill, R., 1951, "A Theory of the Plastic Distortion of a Polycrystalline Aggregate Under Combined Stresses," Philos. Mag., **42**, pp. 414–427.

[9] Ahzi, S., and M'Guil, S., 2005, "Simulation of Deformation Texture Evolution Using an Intermediate Model," Solid State Phenom., **105**, pp. 251–258.

[10] Adams, B. L., Kalidindi, S. R., and Fullwood, D. T., 2008, *Micro Structure Sensitive Design for Performance Optimization,* 2nd ed., BYU Academic Publishing, Provo.

[11] Fullwood, D. T., Niezgoda, S. R., Adams, B. L., and Kalidindi, S. R., 2010, "Mi-crostructure Sensitive Design for Performance Optimization," Progress Mater. Sci., **55**(6), pp. 477–562.

[12] Lekhnitskii, S. G., 1968, *Anisotropic Plates*, 1st ed., Gordon and Breach Science Publishers, New York.

[13] Bunge, H. J., 1982, *Texture Analysis in Materials Science: Mathematical Methods*, Butterworth and Co., London.

[14] Wright, S. I., Adams, B. L., and Kunze, K., 1993, "Application of a New Automatic Lattice Orientation Measurement Technique to Polycrystalline Aluminum," Mater. Sci. Eng., A, **160**(2), pp. 229–240.

[15] Prager, W., and Hodge, P. G., 1968, *Theory of Perfectly Plastic Solids*, Dover, New York.

[16] Chin, G. Y., and Mammel, W. L., 1967, "Computer Solutions of the Taylor Analysis for Axisymmetric Flow," Trans. Met. Soc. AIME, **239**, pp. 1400–1405.

[17] Clausen, B., Leffers, T., Lorentzen, T., Pedersen, O. B., and Van Houtte, P., 2000, "The Resolved Shear Stress on the Non-Active Systems in Taylor/Bishop-Hill Models for FCC Polycrystals," Scr. Mater., **42**, pp. 91–96.

[18] Adams, B. L., Nylander, C., Aydelotte, B., Ahmadi, S., Landon, C., Stucker, B. E., and Ram, G. D. J., 2008, "Accessing the Elastic-Plastic Properties Closure by Rotation and Lamination," Acta Mater., **56**, pp. 128–139.

[19] Kalidindi, S. R., Knezevic, M., Niezgoda, S., and Shaffer, J., 2009, "Representation of the Orientation Distribution Function and Computation of First-Order Elastic Properties Closures Using Discrete Fourier Transforms," Acta Mater., **57**(13), pp. 3916–3923.

[20] Knezevic, M., and Kalidindi, S. R., 2007, "Fast Computation of First-Order Elastic-Plastic Closures for Polycrystalline Cubic-Orthorhombic Microstructures," Comput. Mater. Sci., **39**(3), pp. 643–648.

[21] Van Houtte, P., 1988, "A Comprehensive Mathematical Formulation of an Extended Taylor-Bishop-Hill Model Featuring Relaxed Constraints, the Renouard-Wintenberger Theory and a Strain Rate Sensitivity Model," Textures Microstruct., **8–9**, pp. 313–350.

[22] Kocks, U. F., Tome, C. N., and Wenk, H.-R., 1998, *Texture and Anisotropy: Preferred Orientations in Poly Crystals and Their Effect on Materials Properties*, Cambridge University, New York.